Experimental study of the nature of the 1^- and 2^- excited states in ^{10}Be using the ^{11}Be(p, d) reaction in inverse kinematics

K. Kuhn,[1] F. Sarazin,[1,*] F. M. Nunes,[2] M. A. G. Alvarez,[3] C. Andreoiu,[4] D. W. Bardayan,[5,†] P. C. Bender,[6,‡] J. C. Blackmon,[7] M. J. G. Borge,[8] R. Braid,[1] B. A. Brown,[2] W. N. Catford,[9] C. Aa. Diget,[10] A. DiPietro,[11] T. E. Drake,[12] P. Figuera,[11] A. B. Garnsworthy,[6] J. Gómez-Camacho,[3,13] G. Hackman,[6] U. Hager,[1] S. V. Ilyushkin,[1] E. Nácher,[14] P. D. O'Malley,[1,†] A. Perea,[8] V. Pesudo,[15,§] S. T. Pittman,[5] D. Smalley,[1] C. E. Svensson,[16] O. Tengblad,[8] P. Thompson,[5] C. Unsworth,[6] and Z. M. Wang[4,6]

[1]*Physics Department, Colorado School of Mines, Golden, Colorado 80401, USA*
[2]*Department of Physics and Astronomy, Michigan State University, East Lansing, Michigan 48824, USA*
[3]*Departamento de FAMN, Universidad de Sevilla, Sevilla E-41080, Spain*
[4]*Department of Chemistry, Simon Fraser University, Burnaby, British Columbia V5A 1S6, Canada*
[5]*Oak Ridge National Laboratory, Oak Ridge, Tennessee 37831, USA*
[6]*TRIUMF - Canada's Particle Accelerator Centre, Vancouver, British Columbia V6T 2A3, Canada*
[7]*Department of Physics and Astronomy, Louisiana State University, Baton Rouge, Louisiana 70803, USA*
[8]*Instituto de Estructura de la Materia, CSIC, Madrid E-28006, Spain*
[9]*Department of Physics, University of Surrey, Guildford GU2 7XH, United Kingdom*
[10]*Department of Physics, University of York, York YO10 5DD, United Kingdom*
[11]*INFN, Laboratori Nazionali del Sud, Catania 95123, Italy*
[12]*Department of Physics, University of Toronto, Toronto, Ontario M5S 1A7, Canada*
[13]*Centro Nacional de Aceleradores, Universidad de Sevilla, CSIC, Sevilla E-41092, Spain*
[14]*Instituto de Física Corpuscular, CSIC-Universidad de Valencia, Valencia E-46071, Spain*
[15]*CIEMAT, Centro de Investigaciones Energéticas, Medioambientales y Tecnológicas, Madrid E-28040, Spain*
[16]*Department of Physics, University of Guelph, Guelph, Ontario N1G 2W1, Canada*

(Received 7 May 2021; accepted 8 September 2021; published 1 October 2021)

The nature of the 1^- and 2^- excited states in ^{10}Be is studied using the ^{11}Be(p, d) transfer reaction in inverse kinematics at 10A MeV at TRIUMF ISAC-II, in particular to assess whether either of them can be considered as an excited halo state. The angular distributions for both states are extracted using deuteron-γ coincidences and analyzed using a transfer model taking into account one-step and two-step processes. A good fit of the angular distributions is obtained considering only the one-step process, whereby an inner $p_{3/2}$ neutron of ^{11}Be is removed, leaving the halo neutron intact. Higher-order processes however cannot be rejected. The small spectroscopic factors extracted suggest that the structure of both states is not uniquely halo-like, but rather display a more complex configuration mixing cluster and halo structures. Further insights are limited, as this experiment specifically probed the halo-like (but not cluster-like) $^{11}\text{Be}(1/2^+) \otimes (\nu p_{3/2})^{-1}$ configuration in both states.

DOI: 10.1103/PhysRevC.104.044601

I. INTRODUCTION

Since the discovery of the extended nature of ^{11}Li [1] and its interpretation as a halo nucleus [2], a large number of light (near) drip line nuclei have been found to display similar properties [3]. A halo nucleus is best defined by the extended tail of its probability density distribution arising from the weakly bound valence nucleon(s) found in low angular momentum orbital(s). Traditionally, nuclei displaying halo properties have been identified by measuring their anomalously large spatial extent or conversely their narrow longitudinal momentum distribution through a variety of experimental methods (see [3] and references therein). The concept of halo, however, not only applies to the ground states of nuclei, but can be generalized to loosely bound excited states displaying a strong single-particle nature dominated by low-orbital angular momentum radially extended configurations. To date, a number of excited halo state candidates have been suggested to exist, but demonstrating their halo nature is difficult since it is not possible to apply most experimental techniques available for ground-state studies. Two excited halo states have been firmly

*Corresponding author: fsarazin@mines.edu
†Now at Physics Department, University of Notre Dame, Notre Dame, IN 46556, USA.
‡Now at Physics Department, University of Massachusetts-Lowell, Lowell, MA 01854, USA.
§Now at Instituto de Estructura de la Materia, CSIC, Madrid E-28006, Spain.

shown to exist. The first one is the one-neutron halo $1/2^-$ first excited state in ^{11}Be located about 180 keV below the one-neutron separation energy (S_n) [4,5]. The second one is the one-proton halo $1/2^+$ first excited state in ^{17}F located 105 keV below the one-proton separation energy (S_p) [6]. Among the other candidates, the 2^- state in ^{10}Be (about 550 keV below S_n) has been the subject of numerous experimental and theoretical studies (see [7] and references therein). In this context, there appears to be a solid consensus that both the 1^-_1 and 2^-_1 states (later referred to as 1^- and 2^- respectively) in ^{10}Be are dominated by a $^9\mathrm{Be}(3/2^-) \otimes \nu s_{1/2}$ configuration, but the determination of the halo nature of the more loosely bound 2^- state remains largely elusive not only because of the experimental difficulties cited above, but also because both the 1^- and 2^- states have simultaneously been identified as cluster states [8,9].

Clustering is at the heart of the structure of most states in beryllium isotopes (see [10,11] and references therein) with the states most likely to develop strong clustering expected to be found near and above their relevant cluster thresholds. When describing states in terms of α-α clustering beyond ^{8}Be, one also needs to take into account the role of the extra valence neutron(s) and the concept of nuclear clusters is expanded to one of nuclear molecules. The ground state of ^{9}Be, located 1.57 MeV below the $\alpha + \alpha + n$ threshold, is an example of a nuclear molecule, where the $p_{3/2}$ valence neutron provides the binding energy that prevents the two α particles from dissociating. As we move to the more neutron-rich Beryllium isotopes, the cluster and molecular thresholds migrate to higher energies above the one- or two-neutron separation energies, and their ground states display more compact structures [12], appearing more shell-model-like. Just as this happens, one-neutron and two-neutron halo configurations develop for ^{11}Be and ^{14}Be respectively. It would therefore not be surprising that some states in beryllium isotopes would display hybrid structures born out of the interplay between cluster and molecular configurations on the one hand and halos on the other.

In the particular case of the 1^- and 2^- states in ^{10}Be, we are seeking to probe the halo nature of these states by using the proximity of one-neutron halo ^{11}Be to our advantage. One attractive way indeed to populate the 1^- and 2^- states in ^{10}Be is to use the $^{11}\mathrm{Be}(p, d)$ transfer reaction. In this case, both states may be populated through the transfer of an inner $p_{3/2}$ neutron from the ^{10}Be core, thereby preserving the ^{11}Be halo neutron in the final configuration. Using such reaction, we would expect the spectroscopic factors to reflect the overlap between those states and the ^{11}Be ground-state wave function, including its characteristic one-neutron halo feature. This reaction has been shown to strongly populate excited states around 6 MeV in ^{10}Be. There are four excited states in relatively close proximity from each other in this energy region: a second 2^+_2 at 5958.4 keV, the 1^- at 5959.9 keV, a second 0^+_2 at 6179.3 keV and the 2^- at 6263.3 keV [13]. As a result, until very recently, the states being populated in the $^{11}\mathrm{Be}(p, d)$ reaction could only be inferred due to the lack of energy resolution afforded by experiments relying exclusively on charged-particle detection. A fit of the 6-MeV angular distribution obtained in the first $^{11}\mathrm{Be}(p, d)$ experiment performed at GANIL [14,15] is found to be consistent with a $\ell = 1$ transfer, suggesting that the states being populated are mainly the 1^- and 2^- states through the transfer of an inner $p_{3/2}$ neutron from the ^{10}Be core of ^{11}Be. The summed spectroscopic factor was found to be quite large (1.4), suggesting a strongly dominant $^9\mathrm{Be}(3/2^-) \otimes \nu s_{1/2}$ configuration for both states, consistent with an earlier one-neutron knockout reaction at the National Superconducting Cyclotron Laboratory (NSCL) facility [16].

Recently however, two experiments have extracted smaller spectroscopic factors. First, a $^{11}\mathrm{Be}(p, d)$ experiment run at RCNP at a similar energy yielded a summed spectroscopic factor about two times lower using similar assumptions [17]. Second, a lower-energy $^{11}\mathrm{Be}(d, t)$ experiment performed at ISOLDE-CERN at 2.8A MeV was able to extract individual spectroscopic factors for the states populated at 6 MeV using coincidences between charged-particle and γ-ray detectors [18]. Johansen *et al.* find that the 2^+_2 state in ^{10}Be is also populated together with the 1^- and 2^- states. The sum of the 1^- and 2^- spectroscopic factors [$S = 0.31(11)$ and $S = 0.40(10)$ respectively] is found to be about 0.7, also much lower than [14] and in agreement with [17]. The population of the 2^+_2 is postulated to be due to a two-step process, which may not contribute significantly at higher energies. Given the low energy at which the ISOLDE experiment was performed, the authors caution that their one-step neutron transfer model may not be completely reliable, hence an experiment in an intermediate energy range is warranted to evaluate the spectroscopic factors of the 1^- and 2^- states in particular.

In what follows, we present the results of a $^{11}\mathrm{Be}(p, d)$ transfer reaction at about 10A MeV performed in inverse kinematics at TRIUMF ISAC-II [19] using a combination of charged-particle and γ-ray detectors. In Sec. II, we describe the experimental setup and data analysis. In Sec. III, a short description of the reaction model is provided. In Sec. IV, we present the angular distributions extracted from this work together with their analysis using a single-particle model. Finally, we discuss the results in Sec. V before providing a summary.

II. EXPERIMENTAL SETUP AND DATA ANALYSIS

Given that the energy of the 2^+_2, 1^-, 0^+_2, and 2^- states in ^{10}Be are within 300 keV of each other, it is not possible to separate those states using charged-particle detectors only, hence the need to use deuteron-γ coincidences for proper identification. The assignment of the individual contribution from the 2^+_2 and 1^- states is further complicated since they are less than 2 keV apart. In this context, the $^{11}\mathrm{Be}(p, d)^{10}$Be transfer reaction was performed using a combination of highly segmented charged-particle detectors placed inside the TRIUMF-ISAC Gamma-Ray Escape Suppressed Spectrometer (TIGRESS) [20].

The ^{11}Be beam was produced by impinging a 45 μA 479 MeV proton beam produced by the TRIUMF cyclotron on a tantalum target and extracted using the TRIUMF Resonant Ionization Laser Ion Source (TRILIS) [19]. The beam was then post-accelerated to 9.93A MeV through the ISAC-I and

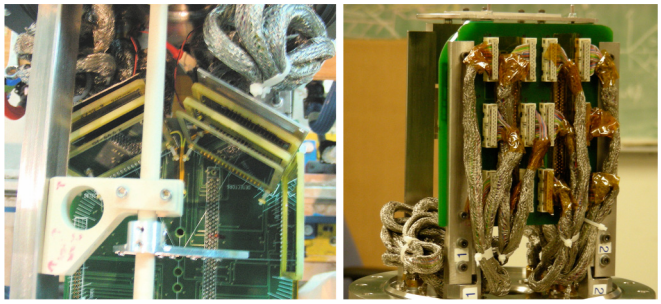

FIG. 1. Left: Charged-particle setup comprising two ΔE_1-ΔE_2-E telescopes and one side detector mounted on a custom-made detector PCB board. Right: The back of the base board supporting the detector PCB with all the connectors taking the signals out of the SHARC vacuum chamber.

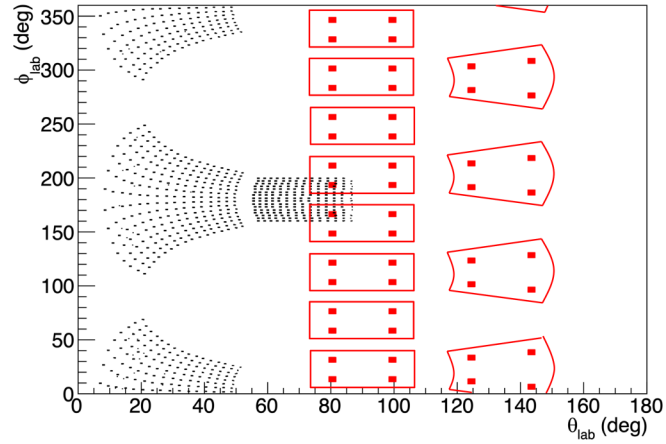

FIG. 2. Nominal angular coverage of the experimental setup. In black, the nominal angular coverage of the charged-particle silicon detectors shown as collections of individual pixels. In red is the nominal angular coverage of the TIGRESS clovers, including the core positions (squares). This figure does not reflect missing channels taken into account in the analysis.

ISAC-II accelerators and delivered to the TIGRESS beam line with an intensity of about 1×10^5 pps, where it impinged a 638 μg/cm^2 CH_2 target located at the center of TIGRESS.

The charged-particle detector setup used in this experiment consisted mainly of two forward silicon telescopes designed to detect and identify deuterons. To minimize the deuteron identification energy threshold, the first element of the telescopes was a thin 40 μm detector. The thicknesses of the other two stages of the left (right) telescope were respectively 295 μm (499 μm) and 500 μm (505 μm). This allowed for the detection and identification of deuterons with energies greater than 2 MeV and up to 14 MeV (17 MeV) in the left (right) telescope respectively. Beside the telescopes, one thick (1 mm) side detector was also used to measure the elastically-scattered protons to determine the entrance channel optical model parameters and overall cross-section normalization. All the detectors used were double-sided silicon strip detectors, except for the last element of the telescopes.

Kinematics considerations were all that was required to identify the elastically scattered protons in the side detector. The charged-particle detectors were mounted inside the vacuum chamber on a set of specially designed multilayered printed circuit boards (PCBs), similar to the ones used in [21]. Figure 1 (left) shows the detectors mounted on the top PCB inside the SHARC [22] vacuum chamber together with the target assembly, and (right) all the connections at the back of the bottom PCB to collect the signals from the detectors.

When used with the SHARC vacuum chamber, the TIGRESS γ-array consists of 12 HPGe detectors with eight high-purity germanium (HPGe) clovers at 90° and four (upstream of the target) at 135° with respect to the beam axis. For this experiment, the TIGRESS array was configured in high-efficiency mode and, given the high-energy γ rays being detected, the signals collected by each clover were read out in addback. The overall laboratory angular coverage of the charged-particle detectors (in black) and the HPGe clovers (in red) is shown in Fig. 2.

Figure 3(a) shows the identification of the deuterons in one of the telescopes. Upon selection, the characteristically folded kinematics of the ^{11}Be(p, d) transfer reaction is clearly visible on Fig. 3(b), where the expected kinematic lines for the states of interest are also shown. Figure 3(c) shows the reconstructed ^{10}Be excitation spectrum and Fig. 3(d) the Doppler-corrected γ-ray spectrum above 1 MeV. Notably absent from the γ spectrum are the $0_2^+ \rightarrow 1^-$ 219.4 keV and $0_2^+ \rightarrow 2_1^+$ 2811 keV transitions. Given the high-efficiency of TIGRESS at 200 keV (about 25% in this configuration), the resolution of the expected peak after Doppler correction and relatively large $0_2^+ \rightarrow 1^-$ branching ratio (34%) [23], the low-energy transition, if present, should have been clearly visible. This indicates that the 0_2^+ state is not (or very weakly) populated. This is consistent with the expectation that the 0_2^+ should not display much single-particle strength [14]. It was also not observed in the ISOLDE (d, t) experiment [18]. All the other expected transitions from the populated excited states in ^{10}Be are clearly seen in the spectrum. As expected, it is not possible to separate the individual contributions to the $(2_2^+, 1^-)$ doublet transitions due to the TIGRESS energy resolution even after Doppler correction.

III. REACTION MODEL

Often, ^{11}Be has been described in a collective core (^{10}Be) + particle (neutron) model (see for example [24]). Based on that, the description of the ^{11}Be(p, d) reaction would typically require a three-body treatment explicitly including the excitation of ^{10}Be in a collective model [25]. However, in the present work, the states being populated in ^{10}Be are essentially single-hole states in the ^{11}Be core. These states are not described in a collective model of ^{10}Be. One could then consider a four-body model $p + (n + n + {}^9\text{Be})$ potentially including core excitation of ^{9}Be. The development of that model is difficult and beyond the scope of this work. Instead, in order to have a practical way to analyze this data, we take a more phenomenological approach. We assume the states in ^{11}Be can be mapped into a collective model. We introduce a dipole (β_1) and a quadrupole (β_2) deformation taking into account the properties of the $1/2^-$ (320 keV) and $5/2^+$ (1783 keV) excited

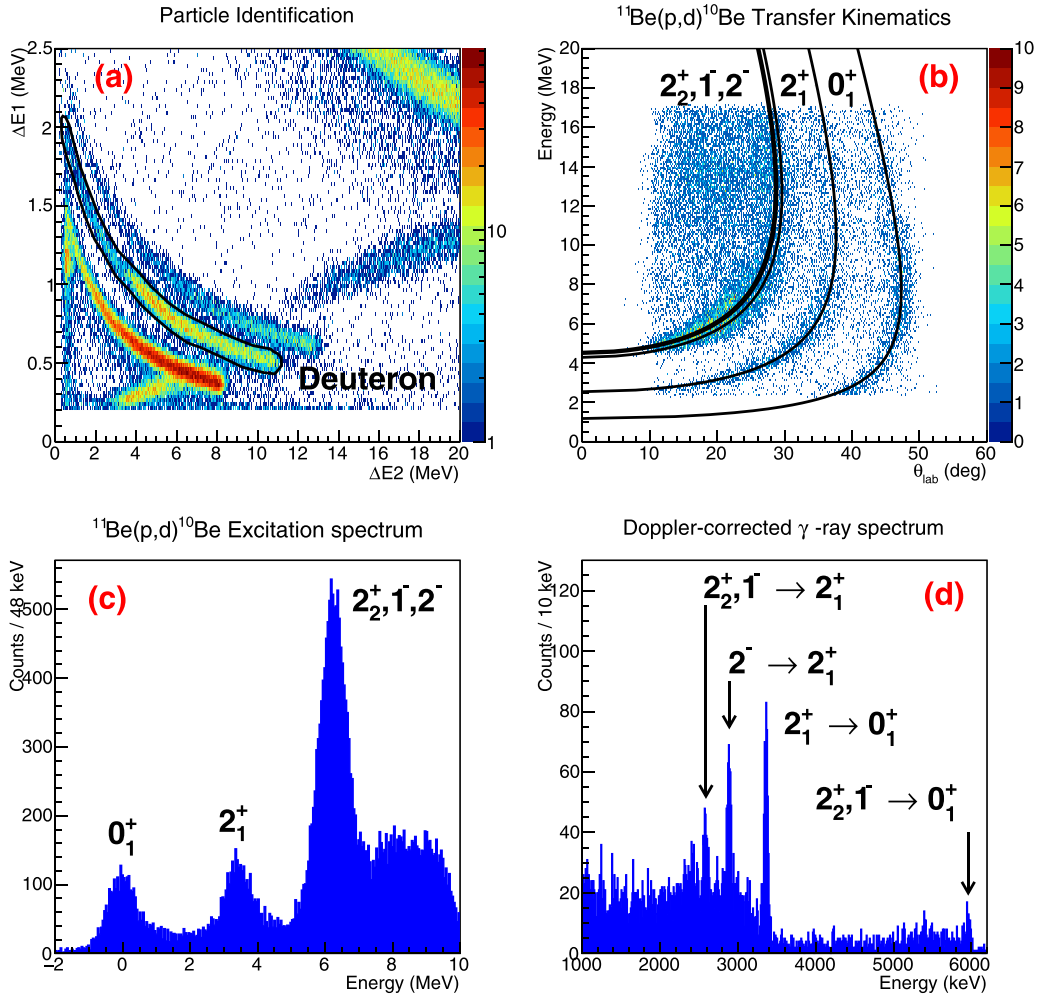

FIG. 3. (a) Particle identification spectrum using the first two stages of the right telescope. The selection of the deuterons is shown as well. (b) Deuteron kinematics from ^{11}Be(p, d) as reconstructed by the telescopes. (c) Corresponding ^{10}Be excitation spectrum with the 6-MeV peak containing contributions from the 2^+_2, 1^-, and 2^- states in ^{10}Be. (d) Doppler-corrected γ-ray spectrum gated on the deuterons in the region of interest with specific transitions highlighted.

states in ^{11}Be. We then couple this system to a single-hole state (corresponding to the neutron-hole in the ^{11}Be core). With this structure model, it is then possible to use standard one-step distorted wave Born approximation (DWBA) to describe the (p, d) reaction and populate the relevant negative parity states. Elastic, inelastic and transfer scattering calculations can then be performed consistently. Calculations are performed with the code FRESCO [26].

IV. RESULTS

A. Elastic and inelastic scattering angular distributions

The ^{11}Be(p, p') elastic and inelastic scattering (to the $1/2^-$ first excited state) angular distributions were extracted from the side detector between $\theta_{\rm lab} = 55^\circ$ and 75°. A gate on the $1/2^- \rightarrow 1/2^+$ 320 keV γ ray was first used to extract the inelastic scattering cross section. The elastic scattering angular distribution was then obtained by subtracting the inelastic scattering contribution from the total angular distribution.

The optical potential for the $p + ^{11}$Be entrance channel was determined by fitting simultaneously both the elastic and inelastic scattering data. The absolute cross sections were obtained by normalizing the elastic angular distribution to the prediction from FRESCO. By varying the optical parameters within reasonable bounds, we found two sets (labeled A and B) of significantly different optical parameters that yielded similar χ^2. This result is not surprising considering the few data points available to constrain the optical potential parameters. While one could argue that the depth of the real potential for set B is too large (see Table I presented later), we decided to keep both sets of parameters to study how they affected the spectroscopic factors extracted from the transfer angular distributions. The fits of the elastic and inelastic scattering angular distributions using model A (solid lines) and model B (dashed lines) can be seen in Fig. 4, where the black circles and red squares show the angular distributions of the elastic and inelastic scattering respectively.

In principle, one would want to normalize the angular distributions on the Coulomb-dominated part of the elastic angular distribution, which is not possible in this case. In the range of θ_{CM} angles covered by this experiment, the Coulomb contribution to the cross section is small and the determination

TABLE I. Optical potential parameters for the entrance and exit channels. Models A and B are the $p + {}^{11}$Be entrance channels resulting from the SFRESCO minimization (see text) and potential D is the $d + {}^{10}$Be exit channel calculated from the RIPL database. Potential depths are in MeV while reduced radii (r_x) and diffuseness (a_x) are in fm. Radii are defined in terms of the reduced radii as $R_x = r_x \times (A_T^{1/3} + A_P^{1/3})$ with A_T and A_P the numbers of nucleons in the target and projectile respectively. Parameters δ_1 and δ_2 are as defined in the text and are in fm.

Label	V_0	r_0	a_0	W_v	W_s	r_s	a_s	δ_1	δ_2
A	27.2	1.76	0.50	2.00	5.45	1.55	0.50	1.67	2.5
B	108.2	1.40	0.81	3.21	4.14	1.40	0.52	1.67	2.5
D	89.0	1.20	0.77	0.0	20.3	1.35	0.62		

of the normalization arises from the constraints placed by the fit of the nuclear potential optical model parameters. As seen in Fig. 4, there is little difference between the angular distributions obtained with model A and model B at small θ_{CM} angles (using the same Coulomb radius $r_C = 1.14$ fm), so we estimate that the systematic error on the normalization coefficient is relatively small, but probably not smaller than 10%. This is taken into consideration in our analysis.

Table I shows the input channel parameters for models A and B together with the $d + {}^{10}$Be exit channel parameters (potential D) extrapolated from the RIPL database [27,28]. The first three parameters (V_0, r_0, a_0) define the real part of the interaction, namely the standard depth, reduced radius and diffuseness for a Woods-Saxon shape. The remaining parameters concern the imaginary component: W_v and W_s for the depths of the imaginary volume term and the imaginary surface term respectively, both with r_s reduced radius and a_s diffuseness. No spin orbit term is included in these calculations as the data does not constrain this part of the interaction, except for potential D for which spin-orbit potential parameters are provided in RIPL. As discussed in Sec. III, we introduce the deformation length parameters $\delta_1 = \beta_1 R$ and $\delta_2 = \beta_2 R$ for

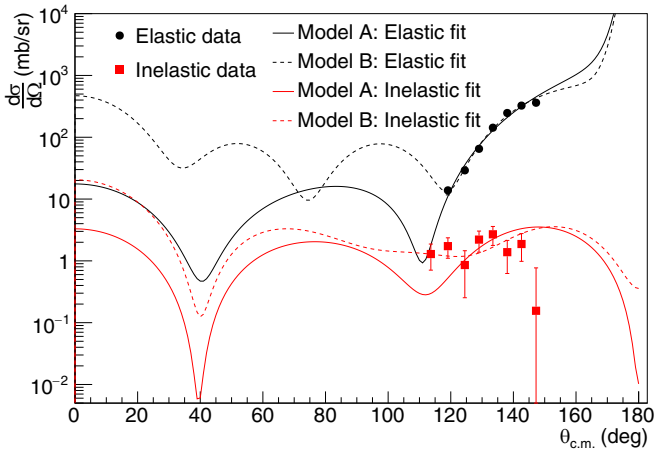

FIG. 4. Elastic (black full circle) and inelastic (red full square) angular distributions (statistical errors only) shown with the best fits obtained using Model A (solid lines) and Model B (dashed lines).

TABLE II. Spectroscopic factors predicted by the shell model considering different ^{11}Be initial configurations.

Excited state	Neutron removed	Initial configuration ^{11}Be$(1/2^+)$	^{11}Be$(5/2^+)$	^{11}Be$(1/2^-)$
2_2^+	$p_{3/2}$			1.107
	$d_{5/2}$	0.007	0.0012	
1^-	$p_{3/2}$	0.693	0.037	
2^-	$p_{3/2}$	0.580	0.345	

^{11}Be (with R the interaction radius). The parameter δ_1 was obtained from the fit of the inelastic angular distribution to the $1/2^-$ 0.320 MeV first excited state (shown in Fig. 4). The parameter δ_2 was then deduced from the δ_2/δ_1 ratio given in [29].

B. Angular distributions of the 1^- and 2^- states in ^{10}Be

As stated earlier, the population of the 1^- and 2^- states in the ^{11}Be(p,d) reaction is believed to mainly proceed through the (one-step) transfer of a $p_{3/2}$ inner neutron from the ^{10}Be core of ^{11}Be leaving the halo neutron in its original $s_{1/2}$ configuration. Hence, the model for these states considers all states to be hole states created from a deformed ^{11}Be nucleus mimicking the halo structure (see Sec. III).

There are other possible contributions, which are expected to be smaller. First, one should in principle account for the fact that the full ^{11}Be wave function includes a small $^{10}\text{Be}(2^+) \otimes \nu d_{5/2}$ component (see for example [30] and references therein), which is difficult to model and would require extensive theoretical work beyond the scope of this work. Second, as pointed out by Johansen *et al.* [18], two-step processes may also contribute at relatively low energy. Perhaps the simplest two-step process to consider for the 1^- and 2^- states is if the transfer proceeds through the ^{11}Be$(5/2^+, 1.783$ MeV) excited state, where the $s_{1/2}$ halo neutron is first promoted to the $d_{5/2}$ orbital. In what follows, we include this possible two-step process in our analysis. As a result, we write the 1^- and 2^- wave functions as

$$\Psi[^{10}Be(1^-/2^-)] = \alpha\psi[^{11}\text{Be}(1/2^+) \otimes (\nu p_{3/2})^{-1}] + \beta\psi[^{11}\text{Be}(5/2^+) \otimes (\nu p_{3/2})^{-1}]. \quad (1)$$

Table II gives the spectroscopic factors extracted from shell model calculations in the $0p1s0d$ space [31] for the single-particle configurations that may contribute to the population of the 2_2^+, 1^-, and 2^- states. As can be seen, the contribution of a two-step process may turn out to be significant, at least for the 2^- state according to this calculation. Interestingly, the shell model calculation also predicts another 2^- state around 9 MeV with a large $^{11}\text{Be}(1/2^+) \otimes (\nu p_{3/2})^{-1}$ configuration. This state has not been observed yet, possibly because of its broad width. The case of the 2_2^+ state will be briefly discussed at the end of this section.

Given the experimental angular distributions deduced for both states, we can find out the optimum α and β parameters by varying the FRESCO spectroscopic amplitudes A_s and A_d of the $^{11}\text{Be}(1/2^+) \otimes (\nu p_{3/2})^{-1}$ and $^{11}\text{Be}(5/2^+) \otimes (\nu p_{3/2})^{-1}$

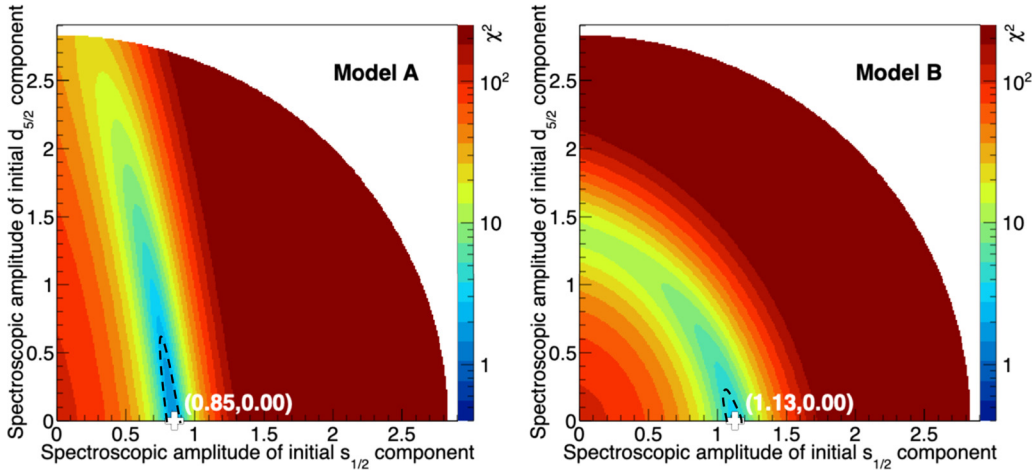

FIG. 5. χ^2 (ndf = 7) surface obtained when varying the spectroscopic amplitudes of the initial $s_{1/2}$ (x axis) and $d_{5/2}$ (y axis) components to fit the 2^- angular distribution for model A (left) and model B (right). The white cross shows the location of the minimum χ^2 and the black dashed line indicates the 1σ limit.

components respectively, with $\alpha = A_s/\sqrt{A_s^2 + A_d^2}$ and $\beta = A_d/\sqrt{A_s^2 + A_d^2}$. The corresponding individual (S_s and S_d) and total spectroscopic (S_{tot}) factors can then also be deduced from the same spectroscopic amplitudes using

$$S_{s/d} = A_{s/d}^2/N, \tag{2}$$

$$S_{\text{tot}} = S_s + S_d, \tag{3}$$

where N is the occupancy number of the $p_{3/2}$ orbital ($N = 4$) prior to the neutron transfer.

To ensure the entire spectroscopic amplitude parameter space is explored, spectroscopic amplitudes $A_{s/d}$ up to about 2.8 (equivalent to spectroscopic factors of about 2) are considered in the χ^2 scan for both 1^- and 2^- states.

In order to extract the angular distributions of the 1^- and 2^- states in ^{10}Be from deuteron-γ coincidences, extensive GEANT4 (G4) [32,33] simulations were necessary to account for the effects due to the kinematics of the reaction and the geometrical efficiency of the experimental setup (including dead strips and edge effects). Prior to extracting the experimental angular distributions, the G4 simulations were thoroughly benchmarked using various fictitious simulated angular distributions. The extraction of the 1^- angular distribution presents the additional challenge of needing to be separated from a contribution of the 2_2^+ state. For this reason, it will be discussed second.

1. 2^-, 6.263 MeV state

The χ^2 exploration of the spectroscopic amplitude phase space, shown in Fig. 5 for both models, yields an optimum solution corresponding to a pure ($\alpha \simeq 1$) ^{11}Be$(1/2^+) \otimes (\nu p_{3/2})^{-1}$ configuration. The χ^2 surfaces however display a strong correlation between A_s and A_d. This can be attributed to the fact that the number of data points in the experimental angular distribution does not allow for a strong discrimination between both processes. While a small contribution from the two-step process cannot be entirely rejected, one would expect the one-step process to dominate the reaction mechanism, which is what is seen here.

Figure 6 shows the angular distribution of the 2^- state together with the fits corresponding to the lowest χ^2 configurations found for models A and B. Shown in black are the data points that were used for the search of the best fit. The extra red data point was extracted for relatively high energy deuterons beyond the fold of the kinematics shown in Fig. 3(b), where the information from two distinct θ_{CM} angles can again be separated from the same θ_{lab} data. The extraction of this data point requires significantly more geometrical corrections based on simulations and could have still contained some residual bias. It is shown in the figure for completeness. This data point is found to be consistent with the best fit of the angular distribution for both models. The extracted spectroscopic factors for all the angular distributions will be discussed together in Sec. V.

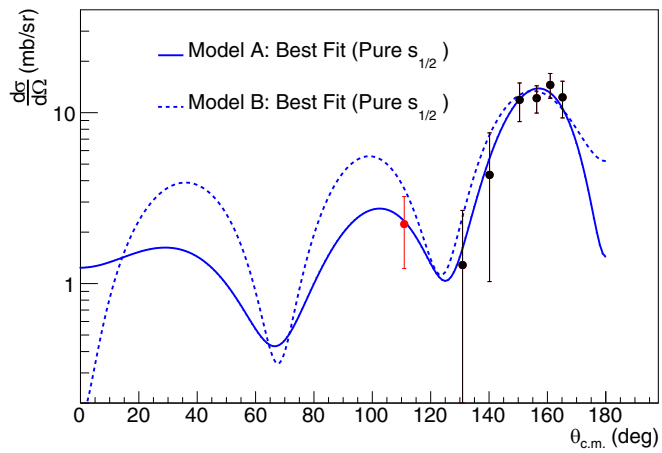

FIG. 6. Best fits obtained for the 2^- angular distribution with model A (solid blue line) and model B (dashed blue line). In this case, the best fits were obtained using a pure $s_{1/2}$ component.

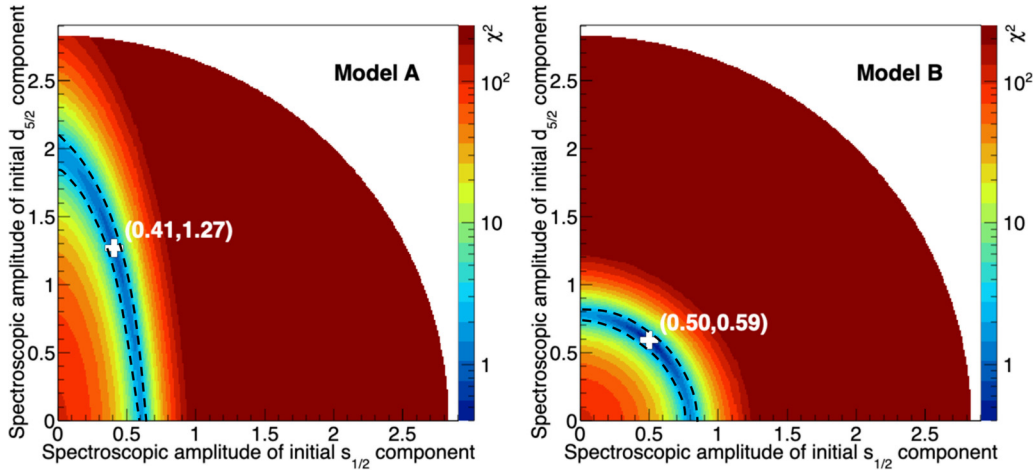

FIG. 7. χ^2 (ndf = 7) surface obtained when varying the spectroscopic amplitudes of the initial $s_{1/2}$ (x axis) and $d_{5/2}$ (y axis) components to fit the 1^- angular distribution for Model A (left) and Model B (right). The white cross shows the location of the minimum χ^2 and the black dashed line indicates the 1σ limit.

2. 1^-, 5.960 MeV state

The 1^- state in ^{10}Be is believed to have a structure similar to the 2^- state, hence the neutron transfer is modeled exactly the same way [see Eq. (1)]. Extracting the angular distribution for the 1^- state does present an additional experimental difficulty due to its close proximity to the 2_2^+ state. Considering the γ-ray intensities extracted for the $(2_2^+, 1^-) \rightarrow 2_1^+$, 2.59 MeV and $(2_2^+, 1^-) \rightarrow 0_1^+$, 5.96 MeV transitions and taking into account the branching ratios of the 2_2^+ and 1^- states [23] to the first 2^+ and ground states, we find that the relative populations of the 2_2^+ and 1^- states are $P_{2_2^+} = 21\%$ and $P_{1^-} = 79\%$ respectively. This means in particular that less than 4% of the $(2_2^+, 1^-) \rightarrow 0_1^+$, 5.96 MeV intensity arises from a contribution from the 2_2^+ state decay. In what follows, we assume this contribution to be negligible.

Given the relatively low efficiency of TIGRESS at 6 MeV (about 3.5% photopeak efficiency), we use a similar approach to Johansen *et al.* in the ISOLDE (d, t) experiment [18], which consists of including part of the Compton background of the 6 MeV photopeak and recalculating the detection efficiency to account for the larger number of events detected. As a minor refinement of the method, we accounted for the fact that the detection efficiency is not constant in the used $E_\gamma =$ 4.8–6.0 MeV range. We therefore weighted the total number of events in the Compton region using 200 keV sections of constant efficiency ($N_{\text{Compton}} = \sum_i \frac{1}{\epsilon_i} N_i$). Equation (4) gives a total efficiency of $\epsilon_{\text{tot}} = 15(2)\%$ in the given energy range for TIGRESS.

$$\epsilon_{\text{tot}} = \epsilon_{5958}\left(1 + \frac{\epsilon_{5958}}{N_{\text{photopeak}}} \sum_i \frac{N_i}{\epsilon_i}\right) \tag{4}$$

where $N_{\text{photopeak}}$ is the number of events recorded in the 5.96 MeV photopeak and ϵ_{5958} is the estimated TIGRESS efficiency at 5958 keV.

To deduce the best fit for the 1^- state angular distribution, we perform a scan of the spectroscopic amplitudes A_s and A_d as done previously for the 2^- state. The result of the scan is shown in Fig. 7. The χ^2 "valleys" obtained for models A and B resemble the ones obtained in the case of the 2^- state. This is not surprising given the fact that both states are expected to share a similar structure. We do see however that the minima are found to be for mixed configurations with nonzero A_d. Considering the 1σ contours, we note that the 1^- angular distribution can still be described satisfactorily by the one-step process only in both models. The 1σ contours reflect the weak constraints placed on the fits due to the small number of data points and the relatively low statistics. Figure 8 shows the angular distribution of the 1^- state deduced from the $1^- \rightarrow 0^+$ transition together with the fits corresponding to the lowest χ^2 configurations found for models A and B (in blue). Also shown in orange are the fits obtained considering only the one-step process (pure s). Similarly to the 2^- case, the search for best fits was carried out using only the black data points, while the red point was excluded due to the large amount of geometrical corrections required. We note in retrospect that,

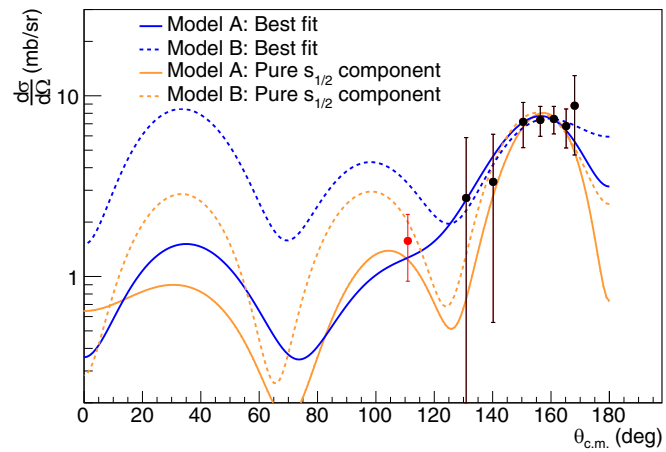

FIG. 8. Best fits obtained for the 1^- angular distribution with Model A (solid blue line) and Model B (dashed blue line). Also shown with solid (dashed) orange lines the fits obtained considering a pure $s_{1/2}$ component for Model A (Model B).

TABLE III. Spectroscopic factors S_x extracted for the 1^- and 2^- states in ^{10}Be using models A and B. For the 1^- state, both the optimum solution and the one resulting from the one-step process only are given. To the statistical-only error bars given in the table, an additional 20% systematic uncertainty needs to be added (see text for details).

State	Model	Reaction	S_s	S_d	S_{tot}
1^-	A	incl. 2-step	0.04[a]	0.40[a]	0.44[a]
	B	incl. 2-step	0.06[a]	0.09[a]	0.15(2)
	A	1-step	0.09(2)		0.09(2)
	B	1-step	0.16(2)		0.16(2)
2^-	A	1-step	0.18(2)		0.18(2)
	B	1-step	0.32(4)		0.32(4)

[a]Large uncertainty.

in the case of model B, the pure one-step process appears to be more favored considering the full angular distribution (including the red data point), while, in the case of model A, the additional data point does not appear to constrain the fit further. The conclusion, similar to the case of the 2^- state, is that the 1^- angular distribution can be described by a one-step process without the need to consider higher order processes (which however cannot be rejected).

3. 2_2^+, 5.958 MeV state

Knowing the 1^- angular distribution, it is in principle possible to extract the 2_2^+ angular distribution from the $(2_2^+, 1^-) \rightarrow 2_1^+$ transition given their relative population and their respective branching ratios to the 2_1^+ state. The 2_2^+ state is expected to exhibit single-particle strength, given its small $B(E2)$ [7]. We did extract an angular distribution for the 2_2^+ state and attempted to fit it using a two-step process, whereas the ^{11}Be halo neutron is first excited to the ^{11}Be$(1/2^-, 0.320$ MeV) excited state (see Table II). The result of this analysis is inconclusive given the large error bars associated with the data points. We do note, however, that the spectroscopic factor required to fit the angular distribution has to be unusually large, possibly suggesting that a different reaction mechanism should be considered to describe the neutron transfer. This is interesting considering that a one-step process (assuming the removal of a $d_{5/2}$ neutron) is not predicted to be significant and appears to also give unsatisfactory results [18].

V. DISCUSSION

Table III summarizes the spectroscopic factors S_x extracted for the 1^- and 2^- states in ^{10}Be. For the 1^- state, they are given considering the one-step process (pure s) only and including a two-step contribution (best fit). For the one-step processes, it is reasonably straightforward to assign an uncertainty on the spectroscopic factor S_s by propagating the spectroscopic amplitude A_s uncertainty obtained from the 1σ contour limits intersecting the x axis in Figs. 5 and 7. For the two-step process cases, the highly correlated nature of the spectroscopic amplitudes A_s and A_d makes it impossible to estimate individual uncertainties on S_s and S_d, and one can only infer that the uncertainties are large. In the case of model B, the serendipitous almost-circular nature of the correlation implies that the total spectroscopic factor S_{tot} is somewhat better constrained, and allows for a reasonable overall uncertainty to be extracted in this particular case only. To the quoted uncertainties in Table III, one needs to add a systematic error of about 20% (propagated to the spectroscopic factors) due to the uncertainties on the elastic scattering normalization, as discussed earlier.

TABLE IV. Spectroscopic factors extracted from this work for the 2^- state (model A / model B) and compared to previous experiments and theoretical predictions.

		Experiment		
This work	Johansen	Jiang	Winfield	Aumann
	[18]	[17]	[14]	[16]
0.18/0.32	0.40	0.7[a]	1.4[a]	0.58
		Theory		
This work	Al-Khalili	Negoita		
	[7]	[34]		
0.58[b]	0.7	0.58		

[a]All 6 MeV excited states.
[b]^{11}Be$(1/2^+)$ initial configuration in Table II.

While the spectroscopic factors obtained for both the 1^- and 2^- states from both models do not always overlap within their uncertainties, they are consistent in pointing to smaller than expected spectroscopic factors and in reasonable agreement with [18]. This confirms the discrepancies observed with the original results obtained by the first ^{11}Be(p, d) experiment, as also pointed out by [17]. These small spectroscopic factors do contrast with other experimental findings and theoretical calculations (see Table IV for the 2^- state), and this appears to call into question the excited halo state nature of both states, and of the 2^- state in particular. As stated before, the reaction mechanism populating both negative parity states involves removing a $p_{3/2}$ neutron from the ^{10}Be core of ^{11}Be, leaving the halo neutron untouched. In this process, it is assumed that the configuration produced corresponds to ^{9}Be$(3/2^-, \text{gs}) \otimes \nu s_{1/2}$. However, in reality we know this mapping is only approximate. For one, there is a d-wave component in the halo of ^{11}Be. In addition, even the s-wave configuration could involve a ^{9}Be$(3/2^-)$ state different from the ^{9}Be$(3/2^-$, gs).

In this respect, the clustered or molecular nature of beryllium isotopes plays a very significant role here. The 1^- and 2^- states in ^{10}Be are part of a group of states, together with the 2_2^+ and 0_2^+ states, that are located simultaneously near the one-neutron separation energy (6.81 MeV) and the $\alpha + {}^6$He energy threshold (7.41 MeV), making them prime candidates for a hybrid structure mixing molecular and halo configurations. There is a vast body of evidence both experimental and theoretical (see [10] and references therein) that the 1^- state can be understood as a molecular bandhead, which second member is the 2^- state. Antisymmetrized molecular dynamics (AMD) calculations have long predicted that those states are built upon two relatively distant α particles bound by two valence neutrons $(p_{3/2}, s_{1/2})$ forming a hybrid σ-π bond [12,35]. Given that the valence neutrons are on separate orbitals, one

expect both states to display single-particle strengths. It is indeed very possible that both the bound negative parity states in ^{10}Be are hybrid states displaying a complex mix of cluster and halo properties. The small spectroscopic factors extracted in this reaction could result from the mismatch between the $^{11}\mathrm{Be}(1/2^+) \otimes (\nu p_{3/2})^{-1}$ and the $^{9}\mathrm{Be}(3/2^-, \mathrm{gs}) \otimes \nu s_{1/2}$ configurations, which very likely display a vastly different amount of clusterization. In this context, the $^{11}\mathrm{Be}(p, d)$ reaction could only provide insights on a well-developed excited halo coupled to a shell-model-like $^{10}\mathrm{Be(gs)} \otimes (\nu p_{3/2})^{-1}$ core. If one assumes that a halo configuration does exist in the 1^- and 2^- states, then the small measured spectroscopic factors are indicative of the poor overlap between the existing core configuration and the one probed by this transfer reaction. This strongly suggests that this core is built upon a more complex and clustered configuration, such as $^{9}\mathrm{Be}(3/2^-, \mathrm{gs})$.

We note here that these hybrid states would not be the only ones to show such a mix of cluster and halo configurations. The unbound 8.81 MeV state in ^{11}Be, sitting very close to the $^{8}\mathrm{Be} + 3n$ and $2\alpha + 3n$ thresholds, likely displays similar properties [23,36–38]. As *ab initio* techniques progress [39], one can expect these will be able to shed light on these issues.

VI. SUMMARY

We have studied the nature of the 1^- and 2^- bound states in ^{10}Be using the $^{11}\mathrm{Be}(p, d)$ reaction at about 10A MeV in inverse kinematics. Spectroscopic factors for both states were extracted and found to be considerably smaller than the combined one extracted from the original $^{11}\mathrm{Be}(p, d)$ experiment. This result is consistent with two recent experiments performed at RCNP and ISOLDE. While the result of our analysis does appear to support a likely dominant $^{9}\mathrm{Be}(3/2^-) \otimes \nu s_{1/2}$ configuration for both states, we suggest that the smaller spectroscopic factors extracted from this experiment do not preclude the existence of an excited halo configuration in both states, but rather point to a more complex core than the $^{10}\mathrm{Be(gs)} \otimes (\nu p_{3/2})^{-1}$ configuration probed with this reaction. With both states simultaneously in close proximity to the $^{6}\mathrm{He} + \alpha$ threshold and to the one-neutron separation energy S_n, they can be identified as "hybrid" states, where the halo neutron also acts as a valence neutron (σ bond) in the molecular framework.

ACKNOWLEDGMENTS

This work was partially supported by the U.S. Department of Energy (DOE) through Grants/Contracts No. DE-FG03-93ER40789 (Colorado School of Mines), No. DE-FG02-96ER40978 (Louisiana State), No. DE-SC0021422 (Michigan State), No. DE-AC05-00OR22725 (Oak Ridge National Laboratory), the National Nuclear Security Administration (NNSA) under the Stewardship Science Academic Alliances program through U.S. DOE Cooperative Agreements No. DE-FG52-08NA28552, and the National Science Foundation under Grant No. PHY-1811815 (Michigan State). This work is also supported by the Natural Sciences and Engineering Research Council of Canada (NSERC), the Canadian Foundation for Innovation (CFI), the British Columbia Knowledge and Development Fund (BCKDF), the Italian National Institute for Nuclear Physics (INFN), the Spanish Ministry of Science and Innovation and FEDER funds under Projects RTI2018-098117-B-C21 and PGC2018-096994-B-C21, and the Spanish Agency of Research (AEI) via Project No. PID2019-104714GB-C21. We would like to thank the staff of the ISAC facility for their work in delivering the ^{11}Be beam. TRIUMF receives federal funding via a contribution agreement through the National Research Council of Canada.

[1] I. Tanihata, H. Hamagaki, O. Hashimoto, Y. Shida, N. Yoshikawa, K. Sugimoto, O. Yamakawa, T. Kobayashi, and N. Takahashi, Phys. Rev. Lett. **55**, 2676 (1985).
[2] P. G. Hansen and B. Jonson, Europhys. Lett. **4**, 409 (1987).
[3] I. Tanihata, H. Savajols, and R. Kanungo, Prog. Part. Nucl. Phys. **68**, 215 (2013).
[4] K. T. Schmitt, K. L. Jones, A. Bey, S. H. Ahn, D. W. Bardayan, J. C. Blackmon, S. M. Brown, K. Y. Chae, K. A. Chipps, J. A. Cizewski, K. I. Hahn, J. J. Kolata, R. L. Kozub, J. F. Liang, C. Matei, M. Matoš, D. Matyas, B. Moazen, C. Nesaraja, F. M. Nunes *et al.*, Phys. Rev. Lett. **108**, 192701 (2012).
[5] K. T. Schmitt, K. L. Jones, S. Ahn, D. W. Bardayan, A. Bey, J. C. Blackmon, S. M. Brown, K. Y. Chae, K. A. Chipps, J. A. Cizewski, K. I. Hahn, J. J. Kolata, R. L. Kozub, J. F. Liang, C. Matei, M. Matos, D. Matyas, B. Moazen, C. D. Nesaraja, F. M. Nunes *et al.*, Phys. Rev. C **88**, 064612 (2013).
[6] R. Morlock, R. Kunz, A. Mayer, M. Jaeger, A. Müller, J. W. Hammer, P. Mohr, H. Oberhummer, G. Staudt, and V. Kölle, Phys. Rev. Lett. **79**, 3837 (1997).
[7] J. Al-Khalili and K. Arai, Phys. Rev. C **74**, 034312 (2006).
[8] W. von Oertzen, Z. Phys. A: Hadrons Nuclei **354**, 37 (1996).
[9] W. von Oertzen, Z. Phys. A: Hadrons Nuclei **357**, 355 (1997).
[10] W. von Oertzen, M. Freer, and Y. Kanada-En'yo, Phys. Rep. **432**, 43 (2006).
[11] M. Freer, Rep. Prog. Phys. **70**, 2149 (2007).
[12] Y. Kanada-En'yo, M. Kimura, and H. Horiuchi, C. R. Phys. **4**, 497 (2003).
[13] D. Tilley, J. Kelley, J. Godwin, D. Millener, J. Purcell, C. Sheu, and H. Weller, Nucl. Phys. A **745**, 155 (2004).
[14] J. Winfield, S. Fortier, W. Catford, S. Pita, N. Orr, J. Van de Wiele, Y. Blumenfeld, R. Chapman, S. Chappell, N. Clarke, N. Curtis, M. Freer, S. Galès, H. Langevin-Joliot, H. Laurent, I. Lhenry, J. Maison, P. Roussel-Chomaz, M. Shawcross, K. Spohr *et al.*, Nucl. Phys. A **683**, 48 (2001).
[15] S. Fortier, S. Pita, J. S. Winfield, W. N. Catford, N. A. Orr, J. van de Wiele, Y. Blumenfeld, R. Chapman, S. P. G. Chappell, N. M. Clarke, N. Curtis, M. Freer, S. Galès, K. L. Jones, H. Langevin-Joliot, H. Laurent, I. Lhenry, J. M. Maison, P. Roussel-Chomaz, M. Shawcross *et al.*, Phys. Lett. B **461**, 22 (1999).
[16] T. Aumann, A. Navin, D. P. Balamuth, D. Bazin, B. Blank, B. A. Brown, J. E. Bush, J. A. Caggiano, B. Davids, T. Glasmacher, V. Guimarães, P. G. Hansen, R. W. Ibbotson, D. Karnes, J. J. Kolata, V. Maddalena, B. Pritychenko, H. Scheit, B. M. Sherrill, and J. A. Tostevin, Phys. Rev. Lett. **84**, 35 (2000).

[17] Y. Jiang, J.-L. Lou, Y.-L. Ye, D.-Y. Pang, J. Chen, Z.-H. Li, Y.-C. Ge, Q.-T. Li, J. Li, W. Jiang, Y.-L. Sun, H.-L. Zang, Y. Zhang, W. Liu, Y.-D. Chen, G. Li, N. Aoi, E. Ideguchi, H. J. Ong, J. Lee *et al.*, Chin. Phys. Lett. **35**, 082501 (2018).

[18] J. G. Johansen, V. Bildstein, M. J. G. Borge, M. Cubero, J. Diriken, J. Elseviers, L. M. Fraile, H. O. U. Fynbo, L. P. Gaffney, R. Gernhäuser, B. Jonson, G. T. Koldste, J. Konki, T. Kröll, R. Krücken, D. Mücher, T. Nilsson, K. Nowak, J. Pakarinen, V. Pesudo *et al.*, J. Phys. G: Nucl. Part. Phys. **44**, 044009 (2017).

[19] J. Dilling, R. Krücken, and G. Ball, Hyperfine Interact. **225**, 1 (2014).

[20] G. Hackman and C. E. Svensson, Hyperfine Interact. **225**, 241 (2014).

[21] V. Pesudo, M. J. G. Borge, A. M. Moro, J. A. Lay, E. Nácher, J. Gómez-Camacho, O. Tengblad, L. Acosta, M. Alcorta, M. A. G. Alvarez, C. Andreoiu, P. C. Bender, R. Braid, M. Cubero, A. Di Pietro, J. P. Fernández-García, P. Figuera, M. Fisichella, B. R. Fulton, A. B. Garnsworthy *et al.*, Phys. Rev. Lett. **118**, 152502 (2017).

[22] C. A. Diget, S. P. Fox, A. Smith, S. Williams, M. Porter-Peden, L. Achouri, P. Adsley, H. Al-Falou, R. A. E. Austin, G. C. Ball, J. C. Blackmon, S. Brown, W. N. Catford, A. A. Chen, J. Chen, R. M. Churchman, J. Dech, D. D. Valentino, M. Djongolov, B. R. Fulton *et al.*, J. Instrum. **6**, P02005 (2011).

[23] C. M. Mattoon, F. Sarazin, C. Andreoiu, A. N. Andreyev, R. A. E. Austin, G. C. Ball, R. S. Chakrawarthy, D. Cross, E. S. Cunningham, J. Daoud, P. E. Garrett, G. F. Grinyer, G. Hackman, D. Melconian, C. Morton, C. Pearson, J. J. Ressler, J. Schwarzenberg, M. B. Smith, and C. E. Svensson, Phys. Rev. C **80**, 034318 (2009).

[24] F. Nunes, I. Thompson, and R. Johnson, Nucl. Phys. A **596**, 171 (1996).

[25] A. Deltuva, A. Ross, E. Norvaišas, and F. M. Nunes, Phys. Rev. C **94**, 044613 (2016).

[26] I. J. Thompson, Comput. Phys. Rep. **7**, 167 (1988).

[27] R. Capote, M. Herman, P. Obložinský, P. Young, S. Goriely, T. Belgya, A. Ignatyuk, A. Koning, S. Hilaire, V. Plujko, M. Avrigeanu, O. Bersillon, M. Chadwick, T. Fukahori, Z. Ge, Y. Han, S. Kailas, J. Kopecky, V. Maslov, G. Reffo *et al.*, Nucl. Data Sheets **110**, 3107 (2009).

[28] Y. Han, Y. Shi, and Q. Shen, Phys. Rev. C **74**, 044615 (2006).

[29] M. S. Hussein and R. Lichtenthäler, Phys. Rev. C **77**, 054609 (2008).

[30] H. T. Fortune and R. Sherr, Phys. Rev. C **85**, 051303(R) (2012).

[31] E. K. Warburton and B. A. Brown, Phys. Rev. C **46**, 923 (1992).

[32] S. Agostinelli *et al.* (GEANT4 Collaboration), Nucl. Instrum. Methods Phys. Res. Sect. A **506**, 250 (2003).

[33] J. Allison *et al.*, Nucl. Instrum. Methods Phys. Res. Sect. A **835**, 186 (2016).

[34] F. Negoita, C. Borcea, F. Carstoiu, M. Lewitowicz, M. G. Saint-Laurent, R. Anne, D. Guillemaud-Mueller, A. C. Mueller, F. Pougheon, O. Sorlin, A. Fomitchev, S. Lukyanov, Y. Penionzhkevich, N. Skobelev, and Z. Dlouhy, Phys. Rev. C **59**, 2082 (1999).

[35] Y. Kanada-En'yo, H. Horiuchi, and A. Doté, J. Phys. G: Nucl. Part. Phys. **24**, 1499 (1998).

[36] F. Sarazin, J. S. Al-Khalili, G. C. Ball, G. Hackman, P. M. Walker, R. A. E. Austin, B. Eshpeter, P. Finlay, P. E. Garrett, G. F. Grinyer, K. A. Koopmans, W. D. Kulp, J. R. Leslie, D. Melconian, C. J. Osborne, M. A. Schumaker, H. C. Scraggs, J. Schwarzenberg, M. B. Smith, C. E. Svensson *et al.*, Phys. Rev. C **70**, 031302(R) (2004).

[37] P. J. Haigh, M. Freer, N. I. Ashwood, T. Bloxham, N. Curtis, P. McEwan, H. G. Bohlen, T. Dorsch, T. Kokalova, C. Schulz, and C. Wheldon, Phys. Rev. C **79**, 014302 (2009).

[38] M. Freer, H. Fujita, Z. Buthelezi, J. Carter, R. Fearick, S. Förtsch, R. Neveling, S. Perez, P. Papka, F. Smit, J. Swartz, I. Usman, P. Haigh, N. Ashwood, T. Bloxham, N. Curtis, P. McEwan, H. Bohlen, T. Dorsch, T. Kokalova *et al.*, Nucl. Phys. A **834**, 621c (2010).

[39] K. D. Launey, T. Dytrych, and J. P. Draayer, Prog. Part. Nucl. Phys. **89**, 101 (2016).